ELSEVIER

Biophysical Chemistry 119 (2006) 219 – 223

Biophysical Chemistry

http://www.elsevier.com/locate/biophyschem

A complementary microscopy analysis of Sticholysin II crystals on lipid films: Atomic force and transmission electron characterizations

José M. Mancheño [a,*], Jaime Martín-Benito [b], José G. Gavilanes [c], Luis Vázquez [d]

[a] *Dpto. Cristalografía Macromolecular, Instituto Rocasolano (CSIC), Serrano 119, 28006 Madrid, Spain*
[b] *Centro Nacional de Biotecnología (CSIC), Campus de la UAM, 28049 Madrid, Spain*
[c] *Dpto. Bioquímica y Biología Molecular I, Facultad de Química, UCM, 28040 Madrid, Spain*
[d] *Instituto de Ciencia de Materiales de Madrid (CSIC), Sor Juana Inés de la Cruz 3, 28049 Madrid, Spain*

Received 23 August 2005; received in revised form 20 September 2005; accepted 20 September 2005
Available online 12 October 2005

Abstract

A new crystal form of the cytotoxin Sticholysin II (StnII) formed on lipid monolayers of 1,2-dioleoyl-*sn*-glycero-3-phosphatidylcholine (DOPC) has been characterized by transmission electron microscopy (TEM) and by tapping mode atomic force microscopy (AFM) under nearly physiological conditions. Both approaches show the existence of single- and double-layered 2D crystals possessing hexagonal symmetry and unit cell dimensions of $a = b = 10$ nm and $\gamma = 120°$. However, single-layered StnII crystals could only be analysed by TEM and double-layered crystals by AFM. Considering the previously known atomic structure of native StnII and that of a tetrameric assembly, a model is proposed for this new crystal form in which StnII conserves its monomeric state upon interaction with the lipid monolayer. These results are in agreement with the existence of the so called M2 state of the actinoporins.

Keywords: Actinoporin; Atomic force; Conformational change; Lipid films; Protein structure; Transmission electron microscopy

1. Introduction

Actinoporins constitute a family of eukaryotic pore-forming proteins (PFPs) (~20 kDa) which are currently under intense study as they represent suitable model systems for analysing protein–membrane interactions at the (sub)-molecular level [1,2]. Whereas there is considerable structural information on prokaryotic PFPs [2–4] the eukaryotic PFPs are much less characterized. Among them equinatoxin II (EqtII) and StnII are the most representative members, with their respective crystal structures being recently solved [5–11]. Both proteins display a very similar β-sandwich fold composed of ten β strands flanked on each side by two short α-helices. Additionally, the structure of StnII complexed with phosphocholine (POC) revealed a putative phospholipid-binding site [10]. Recent biophysical and structural studies have shown that pore-formation by actinoporins proceeds through a mechanism involving large-scale conformational changes at the N-terminus region of the proteins and formation of tetrameric assemblies [10,11]. Nevertheless, the fine structural details involved both in the triggering of the conformational change and its relation with the oligomerization step(s) are yet obscure.

In order to study the structural basis of the protein–lipid interactions underlying the mechanism of actinoporin biological activity, we have analysed by two different microscopy approaches a new crystal form of StnII formed in the presence of lipid monolayers of DOPC. Whereas TEM allows a successful characterization of single-layered 2D StnII crystals, AFM permits an accurate analysis of the surface topography of double-layered StnII crystals.

Abbreviations: StnII, Sticholysin II; EqtII, Equinatoxin II; PFPs, pore-forming proteins; AFM, atomic force microscopy; TEM, transmission electron microscopy.

* Corresponding author. Departamento de Cristalografía Macromolecular, Instituto Rocasolano, Consejo Superior de Investigaciones Científicas, Serrano 119, 28006 Madrid, Spain. Tel.: +34 915619400; fax: +34 915642431.
E-mail address: xjosemi@iqfr.csic.es (J.M. Mancheño).

0301-4622/$ - see front matter © 2005 Elsevier B.V. All rights reserved.
doi:10.1016/j.bpc.2005.09.021

2. Experimental

2.1. Chemicals

Lipids were from Avanti Polar Lipids (Alabaster, AL). Chloroform and methanol were from Merck. All other chemicals were of spectroscopic grade.

2.2. Purification and crystallization of StnII in the presence of lipid films

StnII was isolated from homogenates of whole bodies of *Stichodactyla helianthus* specimens (purchased from Nayeco, Barcelona, Spain) as previously described [5,12,13]. The spectroscopic properties, amino acid composition and permeabilization properties of the obtained protein fully agree with those previously described. The purification protocol involves two chromatographic steps: gel filtration on a Sephadex G-50 column equilibrated in 20 mM ammonium acetate (pH 5.0), and ion-exchange on a CM-cellulose CM-52 column equilibrated in 0.1 M ammonium acetate (pH 5.0). This last chromatography separates two sticholysin isoforms, StnI and StnII, both obtained at sequence grade. All chromatographic steps were performed at 4 °C.

Crystals of StnII in the presence of phospholipid monolayers were obtained essentially as previously described [12]. Briefly, 12–15 μl of a StnII solution in Tris buffer (10 mM Tris–HCl, pH 7.0, containing 0.1 M NaCl and 1 mM EDTA) was added on a Teflon well (3.5-mm diameter and 2.0-mm depth). Immediately, 1 μl of a freshly prepared 1,2-dioleoyl-*sn*-glycero-3-phosphatidylcholine (DOPC) dissolved in chloroform : methanol (2 : 1, v : v) was carefully added to the protein solution. The protein–lipid mixture was incubated at 4 °C in a sealed humid chamber, for different time intervals. Under these conditions, the protein readily adsorbs onto the water/lipid interface [12]. It must be emphasized that we have previously shown that StnII crystallizes in different space groups depending on the crystallization conditions [10,12]. The hexagonal closest packing herein observed represents a new and highly reproducible crystal form.

2.3. Atomic force microscopy

Initially, we considered different AFM supports, which should provide with both an atomically flat surface enabling the visualization of molecular features, and a hydrophobic surface that would permit the lipid–substrate interaction. Thus, we considered glass, freshly cleaved mica and highly oriented pyrolytic graphite (HOPG) as potential AFM substrates. Previously to their use as supporting surfaces, glass and freshly cleaved mica were rendered hydrophobic as described [14]. Positive results were only obtained with freshly cleaved HOPG. Briefly, the crystals were transferred by gently placing a small piece of HOPG on the surface of a well containing the sample; it was incubated for different time intervals (between 30 s and 2 min). After that, its back part was glued on the centre of a Teflon AFM sampleholder. A drop of recording buffer (see below) was immediately added onto the transferred 2D crystals. Because of the hydrophobic character of the Teflon, the drop of the recording buffer poured on top of the StnII/graphite support was confined, allowing the AFM imaging without the o-ring seal. This procedure enabled a larger sampling capability since the sample lateral movements were not limited by this seal.

The AFM used was a Nanoscope IIIa (Digital Instruments, Santa Barbara, CA, USA), equipped with J and D scanners (maximal scan range of ~120 and ~14 μm, respectively). The Si_3N_4 cantilevers herein used had a nominal spring constant of 0.38 N/m and were from Digital Instruments. Unless otherwise indicated all measurements were carried out in freshly prepared and degasified Tris buffer (10 mM Tris–HCl, pH 7.0, containing 0.1 M NaCl and 1mM EDTA) at room temperature, using the fluid cell of the microscope. The samples were imaged with different cantilevers in order to ensure that the imaged structures were not due to tip artefacts. Image acquisition times varied between 2 and 6 min for images with pixel resolutions of 512×512. Tapping mode AFM imaging at drive frequencies close to 9 ± 1 kHz has been used to image the different samples. Because of the extreme softness of the StnII crystals, the tip–sample interaction was minimised during the imaging process. Thus, free amplitude values $A_0 = 0.5–0.7$ V (i.e. 10–20 nm of vibration amplitude) were employed and set points, A, as close as possible to the free oscillation amplitude were employed. These conditions are similar to those employed previously to image by tapping mode AFM in buffer conditions of different protein systems [15].

2.4. Transmission electron microscopy

Transfer of the StnII sample to the electron microscopy grid was performed essentially as previously described [10]. The grids were examined on a JEOL 1200 EX II (100-kV) transmission electron microscope (JEOL Ltd., Tokyo, Japan). Micrographs were taken under low-dose conditions by using the minimum dose focusing system at a calibrated magnification of 39,100× and a nominal underfocus of 2000–4000 Å. The image quality and the crystalline order were evaluated by using CRISP software [16]. The best micrographs were digitized with a PhotoScan TD scanner (Zeiss, Germany) at a resolution of 3.5 Å/pixel and processed with the MRC Image Processing Programs [17] implemented in a Silicon Graphics workstation (Mountain View, CA).

3. Results and discussion

Isolated crystals of StnII were easily located by first imaging large surface areas of the AFM support (up to 50 μm wide). Once selected, we measured a crystal at higher resolution. Fig. 1a is a 6×6 μm^2 AFM image showing one large crystal together with other smaller ones. A sort of depletion region exists close to the central crystal, which is free of the tiny surrounding structures (2–5 nm high) that are probably related to protein aggregates. This clean and depleted surface corresponds likely to the lipid monolayer. The crystal height

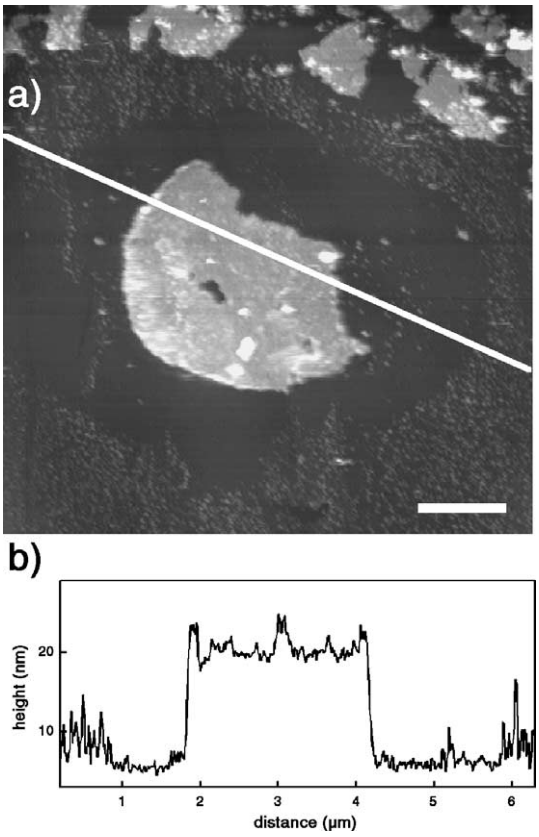

Fig. 1. (a) 6×6 μm^2 AFM topograph showing StnII crystals adsorbed to HOPG after 20 h of incubation and imaged under native conditions (10 mM Tris–HCl, pH 7.0, containing 0.1 M NaCl and 1 mM EDTA). The horizontal bar indicates 600 nm. (b) Surface profile along the white line in image (a).

is in the 13–15 nm range, and the average crystal size is in the 1–2.5 μm range (Fig. 1b). The height of the crystal is clearly larger than that expected for a single-layered 2D crystal of StnII, which according to our X-ray and TEM analyses should be around 4 nm [10]. Although crystals with height close to 4 nm were indeed found, they were too small and imperfect to achieve molecular resolution. The large height value is close to that expected for a double-layered crystal, a scenario which has been observed in other systems [18,19]. Indeed, both single- and double-layered StnII crystals have been found in previous TEM studies (J. Martín-Benito, PhD thesis, Universidad Complutense de Madrid (1998)). Yet, as these studies were only based on a TEM approach, the great complexity of analysing double-layered 2D crystals by this technique precluded its characterization. As shown below, the dual approach herein employed, AFM and TEM, allows us for the first time to characterize both single- and double-layered StnII crystals.

Typical TEM images obtained (Fig. 2a and b) show a well-defined and monocrystalline hexagonal pattern. The basic structure of this 2D crystal can be described as a hexagonal closest packing of cylindrical pore-shaped entities, as assessed by the Fast Fourier Transform (FFT) of the TEM micrograph (Fig. 2c), which provides unit cell dimensions of $a = b = 10$ nm and $\gamma = 120°$. This result clearly shows that this crystal represents a new crystal form.

A higher resolution image of the surface of a double-layered 2D StnII crystal formed in the presence of lipids on HOPG is shown in Fig. 3. The surface exhibits pore-shaped structures assembled into the same packing observed by TEM (Fig. 2). Additionally, it is evident that the crystal surface is not flat but shows protuberances (lighter regions) and deep depressions (darker regions) with a root mean square roughness close to 1 nm. Moreover, different crystalline domains with variable areas (from 1000 to 7000 nm^2) can be distinguished. This result contrasts with the larger average domain size found on the TEM 2D crystals, which is in the 10^6 nm^2 range. However, the FFT corresponding to a given StnII nanodomain imaged by AFM (Fig. 3, inset) correlates well with that obtained from the larger 2D crystals analyzed by TEM.

From the FFT's of the TEM and AFM images we can obtain the respective Fourier maps, in which the corresponding unit cells can be observed (Fig. 4a and b, respectively). The basic hexagonal closest packing structure is observed in both cases. The different contrast of these features observed in both systems is not surprising. It could be due, firstly, to the different systems imaged (single and double layers of StnII) and, secondly, to the different source of contrast of both microscopy techniques (surface topography in AFM and projection of

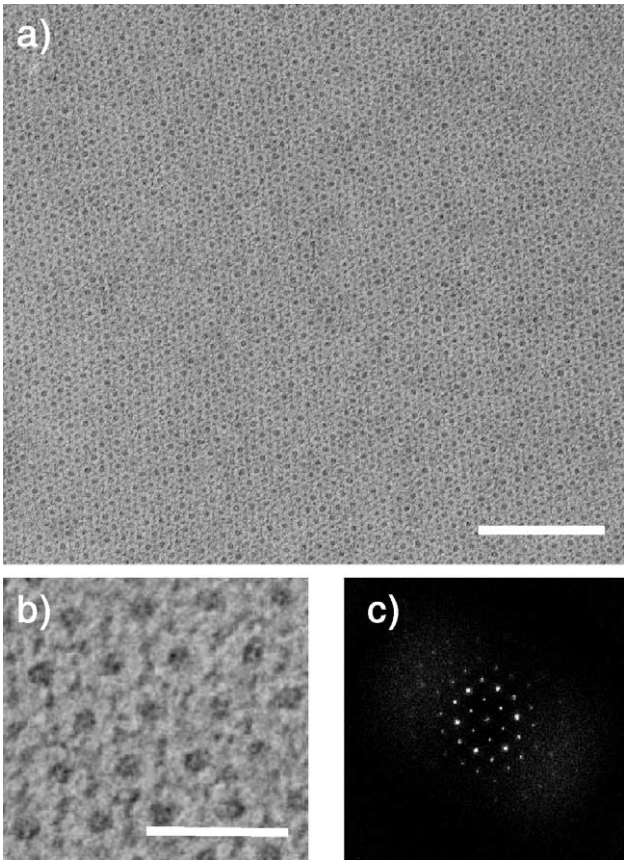

Fig. 2. (a) High-magnification TEM view of a 2D crystal of StnII transferred to an electron microscope grid coated with colodion holey film and recently evaporated carbon. Bar scale, 50 nm. (b) Higher resolution TEM image of the same crystal. Bar scale, 30 nm. Note the presence of pore-shaped structures with inner pores; each pore is surrounded by six small motifs. (c) Two-dimensional Fourier Transform (2D-FT) pattern derived from (a).

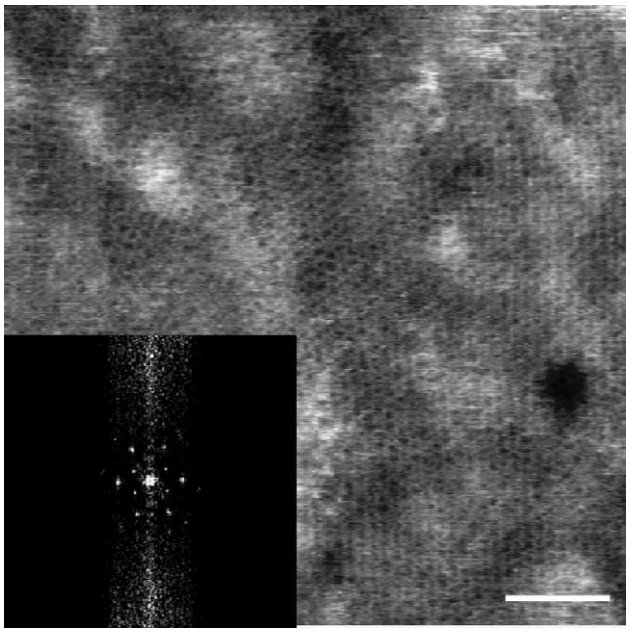

Fig. 3. High-resolution AFM topograph (300×300 nm^2) of the StnII crystal of Fig. 1b showing pore-shaped structures with inner pores assembled in a hexagonal array. Note the different domains of the crystal surface. The horizontal bar indicates 32 nm. *Inset:* Two-dimensional Fourier Transform (2D-FT) pattern derived from a single nanodomain. Note the coincidence of the location of the most intense reflections with those of Fig. 2c. Both patterns are consistent with the same hexagonal lattice ($a = b = 10$ nm, $\gamma = 120°$).

electron density in TEM). Thus, it is evident that the structure of the topmost layer of the AFM StnII crystal keeps a close resemblance with the projection map of the TEM StnII crystal. This matching suggests that the thickness of the crystals observed by AFM corresponds to a double-layer. The fact that their order is perturbed is probably due to the stress induced by the delicate manipulation employed to transferring the crystals to HOPG (see above). Yet, there are obvious differences between both approaches since TEM images of single sheets of StnII reveals that the main pores seem to be isotropically surrounded by protein material giving rise to a quite rich contrast. Also, all the pores look alike. However, in the AFM unit cell, the main pores seem to be connected between them along a preferred direction by globular structures, leading to a sort of preferred stripes or directions. Finally, the pores appear surrounded by four globular structures around 5 nm long and 3 nm wide, in agreement with the dimensions of the individual StnII molecules. Note that the AFM unit cell has been obtained from the FFT analysis of a nanodomain, which implies poorer statistics than the TEM unit cell, which is obtained from microdomains. This poorer statistics may cause that certain weak features, such as the hinted pore connection through a preferred direction, depend on the area analyzed. Next, we verify the existence of four globular structures around the hexagonal close-packed pores by direct high resolution AFM imaging (Fig. 4c). The six main pores are clearly resolved and labelled. A close inspection indicates that they are indeed surrounded by four globular structures. Their average dimensions are close to 5 nm wide and 0.5 nm high as can be seen in the cross-section from pore 1 to 4 (Fig. 4d). In some cases, the tip is not able to resolve two next globular structures, as in the first local maximum of the surface profile. However, in the second maximum it does resolve these two proteins as two local maxima can be distinguished. These limitations can be explained by the intrinsic difficulty in imaging these rather fragile crystals with a multidomain and rough morphology.

Based on recent biophysical and structural studies on both EqtII and StnII it can be proposed a submolecular model of the new crystal form was here described. These studies show that actinoporins suffer large-scale conformational changes in the presence of a water–lipid interface mainly affecting the N-

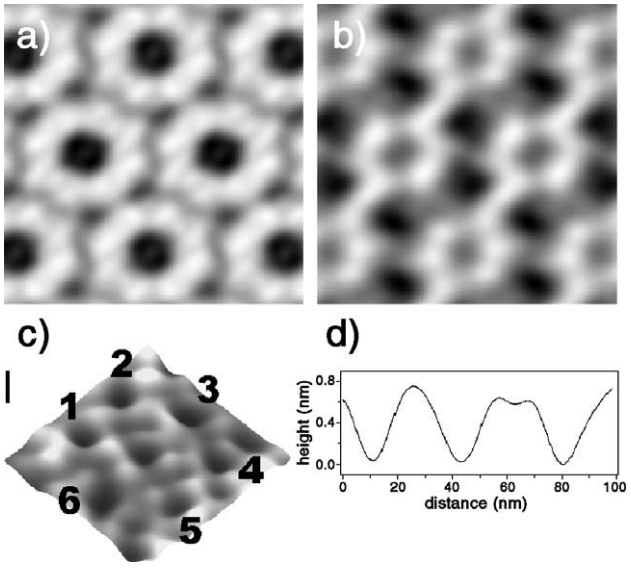

Fig. 4. (a) Fourier map in $p1$ (no symmetry assumed) of the 2D StnII crystal showed in Fig. 2A. (b) Fourier map in $p1$ obtained from a nanodomain of the StnII crystal showed in Fig. 3. (c) High magnification low-pass filtered AFM image (32×32 nm^2) of a unit cell of a StnII crystal measured at low load. The vertical bar indicates 2 nm. Six small cavities labeled 1 to 6 surrounding the central pore are revealed. (d) Cross-section of (c) from pore 1 to 4.

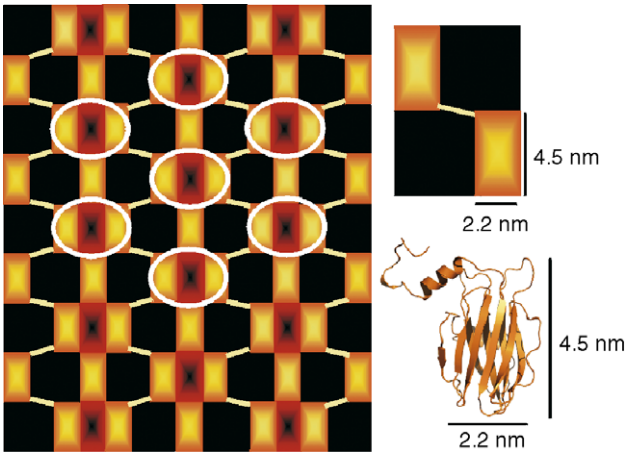

Fig. 5. Schematic model of the StnII crystal formed on lipid monolayers. StnII monomers are shown as orange-yellow rectangles; light yellow bars indicate bridges between monomers, presumably the N-terminal region of StnII. For comparison with Fig. 4A and B, the hexagonal arrangement of protein motifs is highlighted with white ellipses. A ribbon model of StnII is also shown to indicate molecular distances. (For interpretation of the references to colour in this figure legend, the reader is referred to the web version of this article.)

terminal helix [10,11,20]. Our recent studies have shown that tetrameric species of StnII can be readily crystallized in the presence of a lipid interface [10], with each monomer within the protein assembly having suffered a pseudo-rigid body movement of its N-terminal region. As this conformational state is only observed in the presence of lipids, it is conceivable that an initial protein–lipid interaction is required for triggering this conformational transition. From this study, it can be also inferred that protomers finally do not necessarily interact with the lipid monolayer as demonstrated by the existence of an in-plane two-fold screw axis [10]. These two facts would support a putative model for the new crystal forms herein described which considers the crystallization of a conformational state of monomeric StnII with an extended N-terminal region (Fig. 5). This result would be in agreement with previous biochemical results for EqtII which revealed that the most abundant form of the toxin on the membrane is monomeric [21], with an extended N-terminal region [22]. This conformational state has been regarded as M2 state [23]. Finally, although in the model shown in Fig. 5, the bridges between StnII coincide with the weak structural features appearing in the Fourier map from a nanodomain imaged by AFM (Fig. 4b), this conclusion must be taken with caution as stated previously due to the poorer statistics resulting from the small region analyzed. In summary, TEM and AFM microscopies have been *complementary* approaches that have permitted a detailed analysis of a new crystal of StnII in which protein molecules have suffered a conformational change at the N-terminal region.

References

[1] G. Anderluh, P. Maček, Cytolytic peptide and protein toxins from sea anemones (Anthozoa: Actiniaria), Toxicon 40 (2002) 111–124.

[2] M.W. Parker, S.C. Feil, Pore-forming protein toxins: from structure to function, Prog. Biophys. Mol. Biol. 88 (2005) 91–142.

[3] A.P. Heuck, R.K. Tweten, A.E. Johnson, Beta-barrel pore-forming toxins: intriguing dimorphic proteins, Biochemistry 40 (2001) 9065–9073.

[4] E. Gouaux, Channel-forming toxins: tales of transformation, Curr. Opin. Struct. Biol. 7 (1997) 566–573.

[5] V. de los Rıos, J.M. Mancheño, M.E. Lanio, M. Oñaderra, J.G. Gavilanes, Mechanism of the leakage induced on lipid model membranes by the hemolytic protein sticholysin II from the sea anemone *Stichodactyla helianthus*, Eur. J. Biochem. 252 (1998) 284–289.

[6] G. Anderluh, A. Razpotnik, Z. Podlesek, P. Maček, F. Separovic, R.S. Norton, Interaction of the eukaryotic pore-forming cytolysin equinatoxin II with model membranes: ^{19}F NMR studies, J. Mol. Biol. 347 (2005) 27–39.

[7] K. Kristan, Z. Podlesek, V. Hojnik, I. Gutiérrez-Aguirre, G. Guncar, D. Turk, J.M. González-Mañas, J.H. Lakey, P. Maček, G. Anderluh, Pore formation by equinatoxin, a eukaryotic pore-forming toxin, requires a flexible N-terminal region and a stable β-sandwich, J. Biol. Chem. 279 (2004) 46509–46517.

[8] J. Alegre-Cebollada, V. Lacadena, M. Oñaderra, J.M. Mancheño, J.G. Gavilanes, Á. Martínez del Pozo, Phenotypic selection and characterization of randomly produced non-haemolytic mutants of the toxic sea anemone protein sticholysin II, FEBS Lett. 575 (2004) 14–18.

[9] A. Athanasiadis, G. Anderluh, P. Maček, D. Turk, Crystal structure of the soluble form of equinatoxin II, a pore-forming toxin from the sea anemone *Actinia equina*, Structure 9 (2001) 341–346.

[10] J.M. Mancheño, J. Martín-Benito, M. Martínez-Ripoll, J.G. Gavilanes, J.A. Hermoso, Crystal and electron microscopy structures of sticholysin II actinoporin reveal insights into the mechanism of membrane pore formation, Structure 11 (2003) 1319–1328.

[11] Q. Hong, I. Gutiérrez-Aguirre, A. Barlic, P. Malovrh, K. Kristan, Z. Podlesek, P. Maček, D. Turk, J.M. González-Mañas, J.H. Lakey, G. Anderluh, Two-step membrane binding by Equinatoxin II, a pore-forming toxin from the sea anemone, involves an exposed aromatic cluster and a flexible helix, J. Biol. Chem 277 (2003) 41916–41924.

[12] J. Martín-Benito, F. Gavilanes, V. de los Ríos, J.M. Mancheño, J.J. Fernández, J.G. Gavilanes, Two-dimensional crystallization on lipid monolayers and three-dimensional structure of sticholysin II, a cytolysin from the sea anemone *Stichodactyla helianthus*, Biophys. J. 78 (2000) 3186–3194.

[13] V. de los Ríos, J.M. Mancheño, A. Martínez del Pozo, C. Alfonso, G. Rivas, J.G. Gavilanes, Sticholysin II, a cytolysin from the sea anemone *Stichodactyla helianthus*, is a monomer–tetramer associating protein, FEBS Lett. 455 (1999) 27–30.

[14] M. Fritz, M. Radmacher, J.P. Cleveland, M.W. Allersma, R.J. Stewart, R. Gieselmann, P. Janmey, C.F. Schmidt, P.K. Hansma, Imaging globular and filamentous proteins in physiological buffer solutions with tapping mode atomic force microscopy, Langmuir 21 (1995) 3529–3535.

[15] C. Möller, M. Allen, V. Elings, A. Engel, D. Müller, Tapping-mode atomic force microscopy produces faithful high-resolution images of protein surfaces, Biophys. J. 77 (1999) 1150–1158.

[16] S. Hovmöller, CRISP: crystallographic image processing on a personal computer, Ultramicroscopy 41 (1992) 121–135.

[17] R.A. Crowther, R. Henderson, J.M. Smith, MRC: image processing programs, J. Struct. Biol. 116 (1996) 9–16.

[18] A.D. Schenk, P.J.L. Werten, S. Scheuring, B.L. deGroot, S.A. Müller, H. Stahlberg, A. Philippsen, A. Engel, The 4.5 Å structure of human AQP2, J. Mol. Biol. 350 (2005) 278–289.

[19] S. Scheuring, P. Ringler, M. Borgnia, H. Stahlberg, S.A. Müller, P. Agre, A. Engel, High resolution AFM topographs of the *Escherichia coli* water channel aquaporin Z, EMBO J. 18 (1999) 4981–4989.

[20] B.B. Bonev, Y.H. Lam, G. Anderluh, A. Watts, R.S. Norton, F. Separovic, Effects of the eukaryotic pore-forming cytolysin Equinatoxin II on lipid membranes and the role of sphingomyelin, Biophys. J. 84 (2003) 2382–2392.

[21] G. Belmonte, C. Pederzolli, P. Maček, G. Menestrina, Pore formation by the sea anemone cytolysin equinatoxin II in red blood cells and model lipid membranes, J. Membr. Biol. 131 (1993) 11–22.

[22] G. Anderluh, A. Barlic, Z. Podlesek, P. Maček, J. Pugercar, F. Gubensek, M.L. Zecchini, M. Dalla-Serra, G. Menestrina, Cysteine-scanning mutagenesis of an eukaryotic pore-forming toxin from sea anemone. Topology in lipid membranes, Eur. J. Biochem. 263 (1999) 128–136.

[23] P. Malovrh, G. Viero, M. Dalla-Serra, Z. Podlesek, J.H. Lakey, P. Maček, G. Menestrina, G. Anderluh, A novel mechanism of pore formation. Membrane penetration by the N-terminal amphipathic region of equinatoxin, J. Biol. Chem. 278 (2003) 22678–22685.